# Optical Engineering

OpticalEngineering.SPIEDigitalLibrary.org

### Influence of second-order reflections during polarimetric calibration with two wire-grid polarizers

Martin Jan Tauc Wataru Nakagawa Joseph A. Shaw



Martin Jan Tauc, Wataru Nakagawa, Joseph A. Shaw, "Influence of second-order reflections during polarimetric calibration with two wire-grid polarizers," *Opt. Eng.* **58**(8), 082412 (2019), doi: 10.1117/1.OE.58.8.082412.

## Influence of second-order reflections during polarimetric calibration with two wire-grid polarizers

Martin Jan Tauc, Wataru Nakagawa, and Joseph A. Shaw\*

Montana State University, Electrical and Computer Engineering Department, Bozeman, Montana, United States

**Abstract.** In polarimetric instruments, it is often necessary to characterize the polarimetric dependence at various polarization states. Frequently, this is done by placing a polarizer between the instrument and light source. Certain polarizer materials (e.g., wire grids as opposed to polymer-based materials) tend to reflect a significant amount of light, which can cause second-order reflections in the region between the two polarizers. We characterize the reflections using Jones calculus and discuss their significance for polarization instruments. © The Authors. Published by SPIE under a Creative Commons Attribution 4.0 Unported License. Distribution or reproduction of this work in whole or in part requires full attribution of the original publication, including its DOI. [DOI: 10.1117/1.OE.58.8.082412]

Keywords: polarization; reflections; polarimetric calibration; wire grids.

Paper 181708SS received Nov. 29, 2018; accepted for publication Feb. 15, 2019; published online Mar. 12, 2019.

#### 1 Introduction

It is well-known that polarimetric calibrations<sup>1</sup> can be complicated since real polarizers are not ideal. Even seemingly simple measurements quickly become complicated by realities such as low-polarization contrast,2 spectral light leakage,<sup>3</sup> or reflections.<sup>4-6</sup> In this paper, we show experimental measurements and model the effects of multiple reflections in a rotating two-polarizer system. These effects arise in polarimetric calibration measurements that use partially or completely polarized light as a source for determining how a polarimeter responds as a function of the polarization orientation. The orientation of the polarization can be varied electronically with elements such as liquid crystal variable retarders<sup>7,8</sup> or mechanically with a linear polarizer on a rotation stage. 4,9-11 In the latter case, certain polarizers, such as wire grids, may partially reflect the electric field that is parallel to the grids, causing deviations from the ideal case defined by Malus's law.

Reflection from a wire-grid polarizer is a well-known phenomenon; 4-6 however, to our knowledge, the details of multiple reflections have not been discussed in the literature for a two-polarizer setup. Unlike polymer (or other absorptive) polarizers, reflections from wire grids can cause unwanted effects due to the superposition of the electric field. For example, narcissus and reflections of background radiance both must be dealt with in the long-wave (thermal) infrared, where the background is difficult to reduce, or accurately quantify. As a result, some researchers tilt the polarizer so that the reflection comes from a known source. This can be useful for removing unwanted reflections, but it requires a more complicated setup, and it may not always be possible to orient a polarizer at such an angle.

In this paper, we quantify the effects of multiple reflections within a two-polarizer experimental setup in the short-wave infrared (SWIR) spectral band. This analysis is not limited to SWIR wavelengths; rather, it is applicable in bands where a wire-grid polarizer (or other polarizer with reflective

\*Address all correspondence to Joseph A. Shaw, E-mail: joseph.shaw@

properties) has a good contrast ratio and where emissions from optical components are negligible (i.e., outside of the long-wave infrared). By quantifying the multiple reflections within the region between the two polarizers in a polarimetric calibration setup, we can mathematically account for the contributions using simple Jones calculus. Jones calculus is only applicable to completely polarized light, and thus we only consider polarimetric calibrations with completely polarized fields and begin the analysis only after the randomly polarized light passes through the first polarizer. This analysis shows that the first order (or ideal case) of a two-polarizer setup follows Malus's law, and the second-order effect can be quantified with basic linear algebra.

#### 2 Experimental Setup and Results

While conducting a polarimetric calibration to determine the polarimetric dependence of a SWIR polarimeter, we used a halogen light source with an integrating sphere as the randomly polarized input and a rotating polarizer to set the orientation of the polarization (referred to as polarizer 1). The spectral range of the halogen lamp spanned 0.350 to  $2.4 \mu m$  and had a maximum total integrated radiance of  $400~\mathrm{W}~\mathrm{m}^{-2}~\mathrm{sr}^{-1}$ . After light from the halogen source passed through the integrating sphere, the now randomly polarized light exited from a Ø10.16 cm aperture as a diffuse (noncollimated) disk of uniform light. The polarimeter had a fixed polarizer (referred to as polarizer 2) prior to the germanium detector. The absolute positions of either polarizer 1 or polarizer 2 were insignificant (unless the source or detector had some polarization dependence) and so only the relative angular displacement between the two needed be considered. Therefore, polarizer 2 was fixed for simplicity, whereas polarizer 1 was rotated to any arbitrary angle. Polarizer 1 was an aluminum wire grid on UV-grade fused silica with no coating, and polarizer 2 was an aluminum wire grid on Corning Eagle XG with an antireflective coating optimized for 1 to 2  $\mu$ m. Both had an extinction ratio of about 5000:1. A schematic of the setup is shown in Fig. 1, where the first-order interactions are shown as randomly polarized input light filtered by polarizer 1 rotated to angle  $\theta$  relative to  $\hat{x}$ , and then filtered again by the fixed polarizer 2 to transmit the x component to

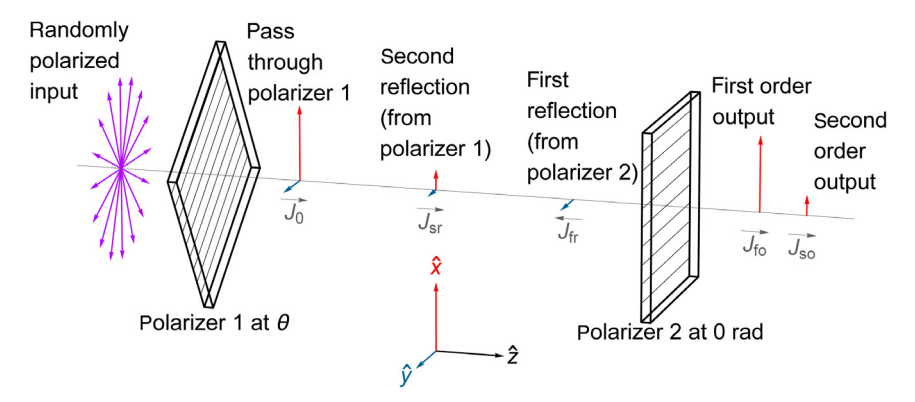


**Fig. 1** Schematic of the setup for the polarimetric calibration used randomly polarized light as the source, polarizer 1, to set the polarization state, and the fixed polarizer 2 prior to the germanium detector (the polarizer lines indicate the wire grids). The electric-field magnitudes are represented by red arrows in  $\hat{\mathbf{x}}$  and teal arrows in  $\hat{\mathbf{y}}$ . The gray arrows (parallel to the optical axis) represent the direction of propagation along the z axis for each transmission or reflection state. The labels under each arrow represent the notation for the initial polarization state ( $J_0$ ), the first reflection ( $J_{\rm fr}$ ), the second reflection ( $J_{\rm sr}$ ), and the first- and second-order outputs ( $J_{\rm fo}$  and  $J_{\rm so}$ , respectively).

the detector. The magnitudes of electric fields from secondorder interactions, discussed below, are shown as the reflected components between polarizer 1 and polarizer 2. Although the schematic shows the wire grids facing the input, we performed experiments with all four permutations of wire grid placement and the same second-order reflections were present regardless of which direction either polarizer was facing. Reflections from the glass substrate likely also contribute to second-order reflections, but our experiments showed these to be much smaller than the wire grid reflections.

Polarizer 1 was rotated from 0 deg to 360 deg in increments of 1 deg using a high-precision rotation stage (Newport RV160CC). The accuracy of the stage was typically better than 0.005 deg. If there was a systematic error in the relative position between the two polarizers, it would

produce a phase shift and could thus be ignored; however, a random error would reduce the goodness of fit. Data from this experiment, which were pedestal subtracted and normalized, are plotted in Fig. 2(a) as black dots, and Malus's law  $I(\theta) = \cos^2(\theta)$  is the blue line. Although the data nominally match the basic structure of the fit, there was a noticeable difference between the two at angles away from the peaks and troughs. By taking the difference between the data and the fit, a systematic error was apparent and is shown in Fig. 2(b) as green squares.

#### 3 Model Using Jones Calculus

The systematic error between the data and fit was due to multiple reflections within the space between polarizer 1 and polarizer 2 and was modeled using Jones calculus. In

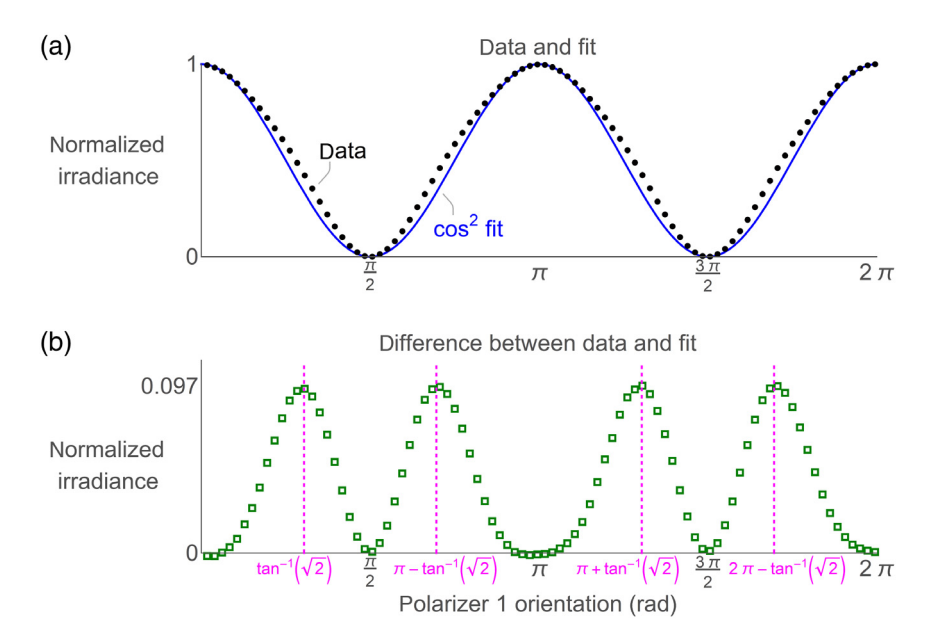


**Fig. 2** (a) The normalized data from the polarimetric calibration are plotted as black dots in the top plot along with the  $\cos^2(\theta)$  fit as a blue line. (b) The difference between the data and fit is shown in the bottom plot as green squares. The difference is systematic with a frequency of about  $2\theta$ . Furthermore, there is an uncharacteristically large valley at  $\pi$  rad, and peaks offset from  $\pi/4$  rad [analysis from Sec. 3 revealed the peaks to be at  $\theta_{\text{max}}$  as defined by Eq. (12)]. To improve readability, only a subset of the experimental data points are plotted.

order to model the reflections—referred to as second-order interactions—we began by modeling the first-order output from the polarizer pair (with no reflections).

Jones calculus can only be applied to completely polarized light, so the analysis began after the randomly polarized input light passed through the first polarizer. This output was defined by the angle of polarizer 1 according to the Jones vector

$$J_0(\theta) = \begin{bmatrix} \cos(\theta) \\ \sin(\theta) \end{bmatrix}. \tag{1}$$

The  $J_0(\theta)$  vector was then manipulated by a series of transmission and reflection matrices that came from the transmission matrix of a general rotated linear polarizer:

$$A_{\rm lin}(\theta) = \begin{bmatrix} \cos^2(\theta) & \cos(\theta)\sin(\theta) \\ \cos(\theta)\sin(\theta) & \sin^2(\theta) \end{bmatrix}. \tag{2}$$

Polarizer 2, fixed at an angle of 0 rad, was simply  $A_{T2} = A_{\text{lin}}(0)$ , so the first-order output from the polarizer pair was calculated using

$$J_{\text{fo}}(\theta) = A_{T2} \cdot J_0(\theta) = \begin{bmatrix} 1 & 0 \\ 0 & 0 \end{bmatrix} \cdot \begin{bmatrix} \cos(\theta) \\ \sin(\theta) \end{bmatrix} = \begin{bmatrix} \cos(\theta) \\ 0 \end{bmatrix}. \tag{3}$$

In an ideal case, the output from the polarizer pair would contain only this first-order term, which follows Malus's law; however, Fig. 2 revealed that there was an additional output, referred to as the second-order output. This effect was dominated by a pair of reflections in the region between the two polarizers. As in the first-order scenario, the initial light through polarizer 1 was where Jones calculus began. The electric field represented by  $J_0(\theta)$  then reflected from polarizer 2 (with reflection matrix  $A_{R2}$ ), then traveled back to polarizer 1 and was reflected from it [with reflection matrix  $A_{R1}$ , Eq. (4)], and finally transmitted through polarizer 2  $(A_{T2})$ . Since wire-grid polarizers may partially reflect the electric-field parallel to the wire-grid orientation, the Jones matrix in Eq. (2) was modified to account for the reflecting (and not transmitting) electric field by rotating  $\theta$  by  $\pi/2$  rad and multiplying by an electric-field reflection coefficient of  $\rho_1$  and  $\rho_2$  (where  $\rho_1^2$  and  $\rho_2^2$  were the reflectances) for polarizer 1 and polarizer 2, respectively. The Jones matrix that represented the reflecting nature of polarizer 1 was

$$A_{R1}(\theta) = \rho_1 A_{\text{lin}}(\pi/2 - \theta)$$

$$= \begin{bmatrix} \rho_1 \sin^2(\theta) & \rho_1 \cos(\theta) \sin(\theta) \\ \rho_1 \cos(\theta) \sin(\theta) & \rho_1 \cos^2(\theta) \end{bmatrix}.$$
 (4)

Similarly, the Jones matrix for the second polarizer was simply  $A_{R2} = \rho_2 A_{\text{lin}}(\pi/2 - 0)$ . Therefore, the second-order Jones vector was

$$J_{so}(\theta) = A_{T2} \cdot A_{R1}(\theta) \cdot A_{R2} \cdot J_{0}(\theta)$$

$$= \begin{bmatrix} 1 & 0 \\ 0 & 0 \end{bmatrix} \cdot \begin{bmatrix} \rho_{1} \sin^{2}(\theta) & \rho_{1} \cos(\theta) \sin(\theta) \\ \rho_{1} \cos(\theta) \sin(\theta) & \rho_{1} \cos^{2}(\theta) \end{bmatrix}$$

$$\cdot \begin{bmatrix} 0 & 0 \\ 0 & \rho_{2} \end{bmatrix} \cdot \begin{bmatrix} \cos(\theta) \\ \sin(\theta) \end{bmatrix}$$

$$= \begin{bmatrix} \rho_{1}\rho_{2} \sin^{2}(\theta) \cos(\theta) \\ 0 \end{bmatrix}. \tag{5}$$

The incoherent nature of the light source required that the irradiance (power per unit area) of each order be calculated as the modulus squared of the Jones vector before adding them together. The first-order output was found, as expected, to follow Malus's law:

$$I_{\text{fo}}(\theta) = ||J_{\text{fo}}(\theta)||^2 = \cos^2(\theta).$$
 (6)

The second-order output was determined by accounting for the first reflection from polarizer 2:

$$I_{fr}(\theta) = ||A_{R2} \cdot J_0(\theta)||^2 = \rho_2^2 \sin^2(\theta), \tag{7}$$

the second reflection (from polarizer 1):

$$I_{\rm sr}(\theta) = ||A_{R1}(\theta) \cdot A_{R2} \cdot J_0(\theta)||^2 = \rho_1^2 \rho_2^2 \sin^2(\theta) \cos^2(\theta), \quad (8)$$

and finally the transmission though polarizer 2

$$I_{so}(\theta) = ||J_{so}(\theta)||^2 = \rho_1^2 \rho_2^2 \cos^2(\theta) \sin^4(\theta).$$
 (9)

The total output, the sum of the first-order and second-order irradiances, was

$$I_{\text{total}}(\theta) = I_{\text{fo}}(\theta) + I_{\text{so}}(\theta) = \cos^2(\theta)[1 + \rho_1^2 \rho_2^2 \sin^4(\theta)],$$
 (10)

and revealed a deviation from Malus's Law. By taking the derivative of the second-order irradiance  $[I_{so}(\theta)]$  in Eq. (9)] with respect to  $\theta$ 

$$\frac{\mathrm{d}I_{\mathrm{so}}(\theta)}{\mathrm{d}\theta} = 4\sin^3(\theta)\cos^3(\theta) - 2\sin^5(\theta)\cos(\theta),\tag{11}$$

and setting it equal to zero and solving for  $\theta$ , we found that the maximum of  $I_{so}(\theta)$  occurred at

$$\theta_{\text{max}} = n\pi + m \tan^{-1}(\sqrt{2}),\tag{12}$$

where n was an integer and m = -1 or 1.

The normalized irradiance of the total output  $I_{\text{total}}(\theta)$ , the first-order output  $I_{\text{fo}}(\theta)$ , the first reflection  $I_{\text{fr}}(\theta)$ , the second reflection  $I_{sr}(\theta)$ , and the second-order output  $I_{so}(\theta)$  are plotted in Fig. 3. The theoretical total output deviated from the first-order output [or  $\cos^2(\theta)$ ] in the same way as the data in Fig. 2. The processes that contributed to the second-order output consisted of two reflections and a final transmission. Polarizer 1 and polarizer 2 in the experimental setup were nearly identical, so our simulations assumed that their field reflectivities were both 90% (i.e.,  $\rho_1 = \rho_2 = 0.90$ ). The first reflection had a  $\pi/2$  rad phase shift from the total and firstorder outputs due to the reflection (and not transmission) from polarizer 1. The second reflection induced the  $2\theta$ dependence because the light was interacting with the  $\theta$ -dependent polarizer 1 again, specifically with the  $\pi/2 - \theta$ component in the reflection instead of the  $\theta$  component from the transmission. Finally, the light transmitted through polarizer 2, which shifted the peaks of the second-order output from odd multiples of  $\pi/4$  rad to  $\theta_{\text{max}}$  and widened the valley at  $\pi$  rad.

The simulated and experimental second-order outputs are shown in Fig. 4 and emphasize that the simulated and real data were nearly identical for a field reflectivity of 90% (or reflectances  $\rho_1^2 = \rho_2^2 = 81\%$ ), which was similar to other reflectance values in the visible band. The troughs were located at multiples of  $\pi/2$  rad with wide troughs at multiples

Tauc, Nakagawa, and Shaw: Influence of second-order reflections...

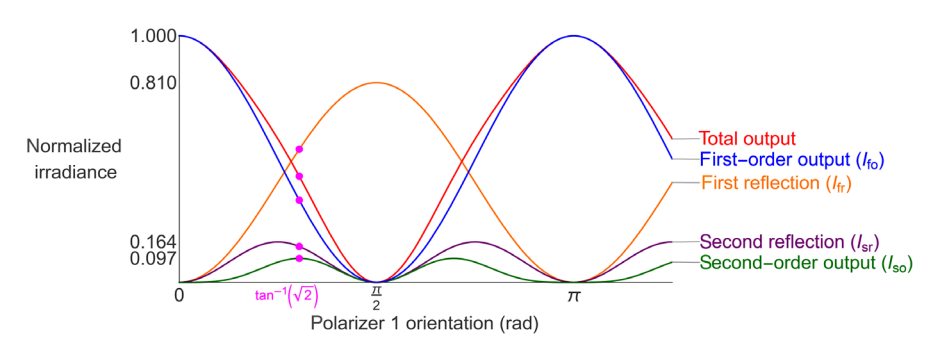


**Fig. 3** The simulated total output (red), first-order output (blue), first reflection (orange), second reflection (violet), and second-order output (green) are shown as a function of polarizer 1 angle  $\theta$ . The location of the first peak in the second-order output is plotted as pink dots on each line to show the results and contributions from the reflections and transmissions. The simulation assumed that  $\rho_1 = \rho_2 = 0.90$ .

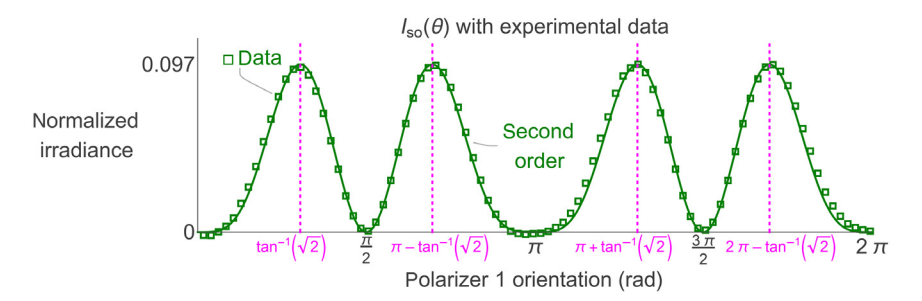


**Fig. 4** The simulated second-order output (line) matched the experimental data (squares) very closely. To improve readability, only a subset of the experimental data points are plotted.

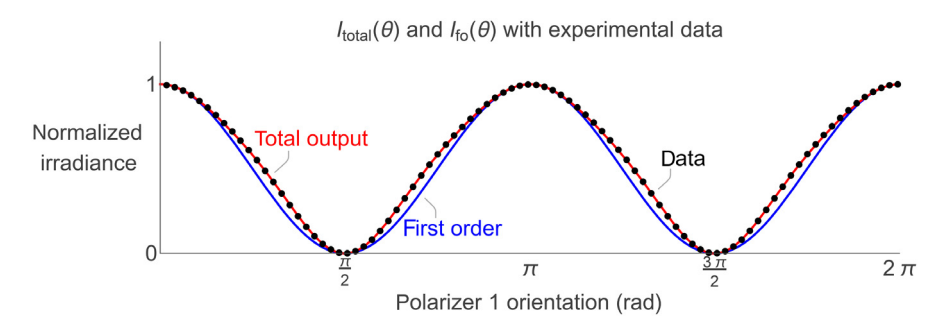


**Fig. 5** The total output (red line) and experimental data (black dots) matched up, suggesting that the total output, Eq. (10), correctly accounted for the first- and second-order effects. The first-order output (blue line) is plotted as a reference to the originally expected result or Malus's law. To improve readability, only a subset of the experimental data points are plotted.

of  $\pi$  rad, and the maxima from the experimental data were located at approximately  $\theta_{max}$ . The field reflectivity value was found by iteratively fitting the experimental data to Eq. (10) and varying the field reflectivity until the root-mean-square error (RMSE) was at a minimum. When simulating the results with the experimentally determined field reflectivity, the maximum irradiance of the simulated second-order output matched the experimental maximum to within 0.17%.

The experimental data and the simulated total output are plotted in Fig. 5, with the first-order output also shown for reference. The inclusion of the second-order output in the calculation of the total shifted the value of irradiance from the first-order output to match the experimental data. The  $r^2$  value (i.e., the ratio of the sum of squares of the regression and total sum of squares) was 0.9999 and the RMSE was 0.0026, indicating a near-perfect fit.

#### 4 Conclusion

In polarimetric experiments (typically calibrations), where two polarizers are on axis with the source and detector, reflections in the space between the two polarizers can have significant impacts on the detected irradiance. Unlike polymer-based polarizers that absorb the electric field parallel to the orientation of the grid, wire-grid polarizers tend to reflect most of this component of the electric field. When the angle between two wire-grid polarizers is not an integer multiple of  $\pi/2$  rad, reflections accumulated in our experiment to the point of altering the output by up to 9.7%. This can cause significant errors when trying to calculate the irradiance accurately and should, therefore, be compensated for. Third-order reflections contribute less than 1% and are ignored in this analysis, although if sensitive applications required this degree of precision, Eq. (5)

could be expanded and thus accommodate any necessary order. Equation (10) can mathematically compensate for the error caused by multiple reflections, thus eliminating the need to tilt or otherwise physically alter the experimental setup.

In addition to mathematically compensating for double reflections, the two-polarizer setup can be used to estimate the on-axis reflectance of wire-grid polarizers. Using Eq. (10) as a fit function and varying the field reflectivity values until the goodness of the fit is optimized will reveal the correct parameter, and thus the reflectance of the wire grid. On-axis reflection values can be difficult to experimentally measure, and so this method can be used to approximate the reflectance. It is likely that  $\rho_1$  and  $\rho_2$  are affected by other parameters in addition to field reflectivity, such as depolarization effects; however, the field reflectivity appears to be the dominant factor.

The reflective properties of wire-grid polarizers must be accounted for in a calibration or measurement. The analysis performed in this paper provides researchers with the necessary equations to compensate for second-order reflections so that both polarizers can remain on-axis. Furthermore, using this analysis as a stepping stone, the theory can be applied to more complicated and sensitive experiments and broaden the usability of the results in this paper.

#### Acknowledgments

This work was funded by NASA EPSCoR under Grant No. NNX14AN40A and Air Force Office of Scientific Research (AFOSR) under Agreement No. FA9550-14-1-0140. The U.S. Government is authorized to reproduce and distribute reprints for governmental purposes notwithstanding any copyright notation thereon. The views and conclusions contained herein are those of the authors and should not be interpreted as necessarily representing the official policies or endorsements, either expressed or implied, of the Air Force Research Laboratory or the U.S. government. The authors declare no conflict of interest.

#### References

- J. S. Tyo et al., "Review of passive imaging polarimetry for remote sensing applications," *Appl. Opt.* 45(22), 5453–5469 (2006).
   J. S. Tyo and H. Wei, "Optimizing imaging polarimeters constructed with imperfect optics," *Appl. Opt.* 45, 5497–5503 (2006).
   J. A. Shaw and M. Vollmer, "Blue sun glints on water viewed through a polarizer," *Appl. Opt.* 56, G36–G41 (2017).

- J. A. Shaw and M. R. Descour, "Instrument effects in polarized infrared images," *Opt. Eng.* 34, 1396–1399 (1995).
   M. H. Smith et al., "Infrared Stokes polarimeter calibration," *Proc. SPIE*
- **4133**, 55–64 (2000).
- 6. C. M. Persons et al., "A proposed standard method for polarimetric calibration and calibration verification," *Proc. SPIE* **6682**, 66820K (2007).
- 7. J. M. Bueno, "Polarimetry using liquid-crystal variable retarders: theory and calibration," J. Opt. A: Pure Appl. Opt. 2(3), 216-222 (2000).
- P. Li and J. S. Tyo, "Experimental measurement of optimal polarimeter systems," *Proc. SPIE* 5158, 103–112 (2003).
   S. B. Powell and V. Gruev, "Calibration methods for division-of-focal-plane polarimeters," *Opt. Express* 21, 21039–21055 (2013).

- Z. Chen, X. Wang, and R. Liang, "Calibration method of microgrid polarimeters with image interpolation," *Appl. Opt.* 54, 995–1001 (2015).
   N. J. Pust and J. A. Shaw, "Dual-field imaging polarimeter using liquid crystal variable retarders," *Appl. Opt.* 45, 5470–5478 (2006).
   X. J. Yu and H. S. Kwok, "Optical wire-grid polarizers at oblique angles of incidence," *J. Appl. Phys.* 93, 4407–4412 (2003).

Martin Jan Tauc received his BS degree in physics and mathematics from the University of Oregon and his MS degree in electrical engineering from Montana State University. He is currently a PhD candidate in electrical engineering at Montana State University with a focus on optics and photonics. His current research is on passive polarimetric measurements of the atmosphere.

Wataru Nakagawa received his BS degree in physics from Stanford University and his MS and PhD degrees in electrical and computer engineering (applied physics) from the University of California, San Diego, La Jolla, California. He is currently an associate professor in the Department of Electrical and Computer Engineering at Montana State University, Bozeman, Montana. His research interests include near-field optical effects in photonic structures and interdisciplinary applications of nanostructured optical devices.

Joseph A. Shaw received his BS degree in electrical engineering from the University of Alaska, his MS degree in electrical engineering from the University of Utah, and his PhD and MS degrees in optical sciences from the University of Arizona. He is a director of the Optical Technology Center and a professor of optics and photonics and electrical engineering at Montana State University, Bozeman, Montana. His research is developing optical remote sensing systems. He is a fellow of OSA and SPIE and is the recipient of the 2019 G. G. Stokes Award from SPIE.